The International Journal of Advanced Manufacturing Technology (2019) 101:1715–1724
https://doi.org/10.1007/s00170-018-3086-3

ORIGINAL ARTICLE

Single-axis driven measurement method to identify position-dependent geometric errors of a rotary table using double ball bar

Shuang Ding[1] · Weiwei Wu[1] · Xiaodiao Huang[2] · Aiping Song[1] · Yifu Zhang[1]

Received: 28 June 2018 / Accepted: 19 November 2018 / Published online: 24 November 2018

Abstract
With the development of error compensation technology, reliability and stability of error identification deserve much attention. And rotary axis errors of five-axis machine tool are the main error sources which result in machining inaccuracy. Hence, a new method for position-dependent geometric error (PDGE) identification of a rotary table using double ball bar was proposed in this paper. Especially, only the targeted rotary table was driven during the ball bar test, which can reduce the impact of interference error sources. During the measurement, the ball on the spindle holds still, and the ball on the rotary table rotates around the rotation axis. There are three mounting positions of magnetic socket on the rotary table. Total six measurement procedures of cone test are executed to obtain enough measuring results by setting different positions of magnetic socket ball. These measuring results are used to construct the identification model based on homogeneous transformation matrix (HTM). The impact of installation errors of the double ball bar on identified results was analyzed. The uncertainty of identified errors could be reduced with the single-axis driven and the installation parameter optimization. At last, testing experiments on a five-axis machine tool were conducted to verify the proposed method. The results confirm that the method is an effective way to identify PDGEs of a rotary axis, and the accuracy of identified results is improved.

Keywords Geometric error identification · Double ball bar · Rotary axis · Five-axis machine tool

1 Introduction

Five-axis machine tool is one of the most important equipment to manufacture complex sculptured surfaces and challenging features, which required higher efficiency and accuracy in modern manufacturing [1]. Rotary axis is equipped on the five-axis machine tools and is an essential component to increase orientation degrees of freedom between the workpiece and the tool. Its accuracy is of great importance for manufacturing high-quality part. The geometric errors of rotary axis are repeatable, measurable, and are the major error sources of machining inaccuracy of five-axis machine tools [2]. Geometric error compensation of rotary axis is an effective method to guarantee high accuracy with low cost. And beautiful methodology for measuring the geometric errors of rotary axis is the foundation to achieve high-performance error compensation. Therefore, it is necessary to research the efficient, accurate, and low-cost method for measuring the geometric errors of rotary axis.

Some instruments, such as laser tracker [3, 4], touch trigger probe [5–9], laser interferometer [10], R-test [11, 12], 6-DOF laser system [13], double ball bar [14, 15], and corresponding strategies have been studied to measure and identify the geometric errors of rotary axis. These methods were verified useful for geometric error tracing of rotational axis. However, many researches are limited by the test condition. The laser tracker is expensive that fewer researchers or machine tool users can get. R-test and 6-DOF laser system need special time-consuming design and manufacture. Also, the touch-trigger probe is depended on the machine tool vendors, equipped or not. And the measurement effect of laser interferometer is observably influenced by the skillful operator and the environment, whereas the double ball bar has the advantages of easy installation, stable measurement, and low cost. Hence, the user free and inexpensive commercial double ball bar is widely studied in the geometric error measurement of rotary axis.

✉ Shuang Ding
dingshuang11@163.com

[1] College of Mechanical Engineering, Yangzhou University, Yangzhou 225127, Jiangsu, People's Republic of China

[2] School of Mechanical and Power Engineering, Nanjing TECH University, Nanjing 211816, Jiangsu, People's Republic of China

The double ball bar was usually used for circular test to evaluate the volumetric performance of machine tools [16–18], including geometric errors, dynamic errors, servo mismatch, and backlash. Recently, the ball bar is developed as an especial displacement sensor to measure the distance change between the two precision balls. The length deviations of the double ball bar are collected to identify the geometric error sources based on the error model. In the early days, simultaneous control of multiple axes was adopted to measure the geometric error of rotary axis conveniently [19]. Zhu et al. [20] proposed a method to identify six geometric errors of a rotary axis with the rotation tool center point (RTCP) function; the three linear axes were driven along with the rotary axis simultaneously. Chen et al. [21, 22] proposed a method to measure and identify the position-independent and position-dependent geometric errors of rotary axis. The deviations of the ball installed on the rotation axis were measured in the three coordinate directions with serial of two linear axes controlled circular paths. Those methods can effectively measure and identify the geometric errors of rotary axis. However, the errors of non-targeted motion axes are often ignored or are supposed to have little impact on the measuring results, which will decrease the measuring accuracy. In addition, multi-axis motion will increase the complexity of movement path and will lower the test efficiency.

Therefore, to reduce the influence of non-targeted motion axes (especially the three linear axes) on the measuring results, different strategies and motion trajectories with only targeted rotation axis rotating have been studied using the double ball bar. Obviously, the ultimate goal of the ball bar test on rotary axis is to identify geometric errors accurately as many as possible with less synchronous control axes and less installation times. For position-independent geometric errors of rotary axis, Jiang et al. [23] proposed a method to detect position-independent geometric errors of rotary axis with single-axis driven based on circular cone trajectory. Lee et al. [24, 25] utilized two parallel circular measurement paths to identify the two offset and two squareness errors of a rotary axis involving single-axis control during the measurement. For PDGE of rotary axis, Xiang et al. designed five testing patterns to measure five PDGEs of a rotary axis with three installations of the magnetic socket [26]. Optimization of installation parameters and the analysis of installation errors of ball bar were lacked in the existing method.

This paper proposed a new method to measure and identify PDGEs of a rotary table with six cone tests. Three installation locations of magnetic socket and two kinds of rod length were designed to collect deviation data. During the measurement, only the targeted rotary table rotates, which reduces the unnecessary interference of other error sources. Sensitivity analysis of the installation error was presented to guide the measurement process. The installation parameters were optimized in the reasonable range according to the analysis results. Finally, experiments were carried out on a five-axis machine tool to detect and to verify the proposed method.

2 Ball bar test patterns with single-axis driven

The double ball bar is a precision instrument to measure the relative displacement between the two balls. As shown in Fig. 1, there are two magnetic sockets in the ball bar measurement system. One is set on the rotary table, named “ball 1” and another is clamped by the tool holder on the spindle, named “ball 2”. The two balls of the double ball bar are installed on the ball bowls of the magnetic sockets. During the measurement, only the targeted rotation axis C rotates, and the length change of the double ball bar is recorded to identify five PDGEs.

Seen in Fig. 1, the initial fixed coordinate system (IFCS) of the rotary table is defined on the upper surface of the rotary table. The origin of the coordinate system is located at the intersection point o_C of C-axis and the table surface. H_0 represents the height from the rotary table to the center of “ball 1.” H_1 and H_2 respectively denote the distance between the centers of the two balls in the z-axis direction with different rod length. R denotes the installation radius of “ball 1” from the ideal rotation axis line.

The distance change between “ball 1” and “ball 2” can be modeled as the function of the PDGE based on HTM. Each combined position of “ball 1” and “ball 2” can establish an equation. To identify the five PDGEs, five equations are needed at least. Three installation locations of “ball 1” and two corresponding positions of “ball 2” are set with the extension bar, thereby six equations can be founded. The identification model, measuring procedure, and the experiments will be described in detail in the following sections.

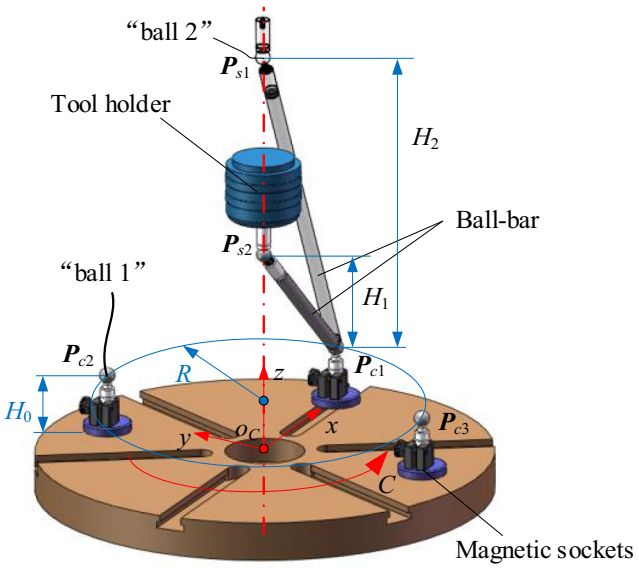

Fig. 1 Cone test of double ball bar measurement

3 Geometric error identification model of the rotary table

The PDGEs $[\delta_x(C), \delta_y(C), \delta_z(C), \varepsilon_x(C), \varepsilon_y(C), \varepsilon_z(C)]^{\mathrm{T}}$ (see in Fig. 2) after rotating an angle C can be defined as three translation errors and three angular errors. They are the functions of the rotation position C. To simplify the expressions, let $[\delta_x, \delta_y, \delta_z, \varepsilon_x, \varepsilon_y, \varepsilon_z]^{\mathrm{T}}$ denote $[\delta_x(C), \delta_y(C), \delta_z(C), \varepsilon_x(C), \varepsilon_y(C), \varepsilon_z(C)]^{\mathrm{T}}$ in the following sections of this paper.

The coordinate system $o_C(0)$–$x_{C0}y_{C0}z_{C0}$ is the IFCS of the rotary axis; its coordinate direction is in accordance with the machine coordinate system o_R-$x_Ry_Rz_R$. $o_C(C)$–$x_Cy_Cz_C$ represents the ideal rotation coordinate system and $o_C'(C)$-$x_C'y_C'z_C'$ denotes the actual rotation coordinate system considering PDGEs.

The mounting positions of the center of "ball 1" and "ball 2" are $\boldsymbol{P}_c$ and $\boldsymbol{P}_s$, respectively. Because of the PDGEs, $\boldsymbol{P}_c$ will deviate from its ideal position after rotating an angle C. The ideal position of $\boldsymbol{P}_c$ after rotating an angle C in IFCS can be calculated as:

$$P_c(C) = M_C[x_{c0}, y_{c0}, z_{c0}, 1]^T \tag{1}$$

$M_C$is the ideal HTM of C-axis motion. (x_{c0}, y_{c0}, z_{c0}) denotes the coordinate of "ball 1" in the IFCS. Let $c_C = \cos(C)$, $s_C = \sin(C)$, $M_C$can be expressed as

$$M_C = \begin{bmatrix} c_C & -s_C & 0 & 0 \\ s_C & c_C & 0 & 0 \\ 0 & 0 & 1 & 0 \\ 0 & 0 & 0 & 1 \end{bmatrix}$$

The actual position of $\boldsymbol{P}_c$ after rotating an angle C in IFCS considering PDGEs can be given as:

$$P_c'(C) = M_C'[x_{c0}, y_{c0}, z_{c0}, 1]^T \tag{2}$$

M_C' is the real HTM considering geometric errors of C-axis motion. And M_C' can be calculated as [27].

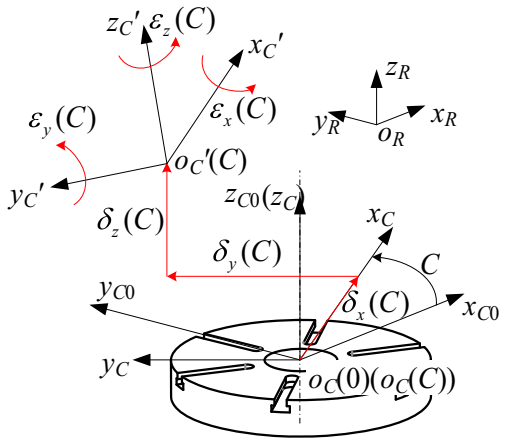

Fig. 2 PDGEs of rotary axis C

$$M_C' = \begin{bmatrix} c_C - \varepsilon_z s_C & -s_C - \varepsilon_z c_C & \varepsilon_y c_C + \varepsilon_x s_C & \delta_x c_C - \delta_y s_C \\ s_C + \varepsilon_z c_C & c_C - \varepsilon_z s_C & \varepsilon_y s_C - \varepsilon_x c_C & \delta_y c_C + \delta_x s_C \\ -\varepsilon_y & \varepsilon_x & 1 & \delta_z \\ 0 & 0 & 0 & 1 \end{bmatrix}$$

And then the three positional errors of "ball 1" can be calculated by

$$[\Delta x_c, \Delta y_c, \Delta z_c, 0]^T = P_c'(C) - P_c(C) \tag{3}$$

Expanding Eq. (3), the positional errors of "ball 1" can be represented by the linear combination of the geometric errors of the rotary table.

$$\begin{cases} \Delta x_c = c_C\delta_x - s_C\delta_y + z_{c0}s_C\varepsilon_x + z_{c0}c_C\varepsilon_y - (x_{c0}s_C + y_{c0}c_C)\varepsilon_z \\ \Delta y_c = s_C\delta_x + c_C\delta_y - z_{c0}c_C\varepsilon_x + z_{c0}s_C\varepsilon_y + (x_{c0}c_C - y_{c0}s_C)\varepsilon_z \\ \Delta z_c = \delta_z + y_{c0}\varepsilon_x - x_{c0}\varepsilon_y \end{cases} \tag{4}$$

Transform Eq. (4) into matrix form.

$$\begin{bmatrix} \Delta x_c \\ \Delta y_c \\ \Delta z_c \end{bmatrix} = \begin{bmatrix} c_C & -s_C & 0 & z_{c0}s_C & z_{c0}c_C & -x_{c0}s_C - y_{c0}c_C \\ s_C & c_C & 0 & -z_{c0}c_C & z_{c0}s_C & x_{c0}c_C - y_{c0}s_C \\ 0 & 0 & 1 & y_{c0} & -x_{c0} & 0 \end{bmatrix} \begin{bmatrix} \delta_x \\ \delta_y \\ \delta_z \\ \varepsilon_x \\ \varepsilon_y \\ \varepsilon_z \end{bmatrix} \tag{5}$$

During the test, only the positional errors of "ball 1" along the ball bar axis can cause the length change. Hence, at a specific measurement angle C, the following equations can be obtained:

$$\begin{cases} n(C) = \dfrac{P_c(C) - P_s}{\|P_c(C) - P_s\|} \\ \Delta L(C) = (\Delta x_c, \Delta y_c, \Delta z_c) \cdot n(C) \end{cases} \tag{6}$$

where, $\boldsymbol{n}(C)$ represents the unit vector connecting $\boldsymbol{P}_s$ (x_s, y_s, z_s) to $\boldsymbol{P}_c(C)$ $(x_c(C), y_c(C), z_c(C))$ at the measurement angle C. $\Delta L(C)$ is the length change obtained from the double ball bar.

Substituting Eq. (5) into Eq. (6), then

$$\begin{bmatrix} -x_sc_C - y_ss_C + x_{c0}; \\ -y_sc_C + x_ss_C + y_{c0}; \\ z_{c0} - z_s; \\ (y_sc_C - x_ss_C)z_{c0} - z_sy_{c0}; \\ z_sx_{c0} - (y_ss_C + x_sc_C)z_{c0}; \\ (x_{c0}s_C + y_{c0}c_C)x_s \\ -(x_{c0}c_C - y_{c0}s_C)y_s \end{bmatrix}^T \begin{bmatrix} \delta_x \\ \delta_y \\ \delta_z \\ \varepsilon_x \\ \varepsilon_y \\ \varepsilon_z \end{bmatrix} = \Delta L(C)\|P_c(C) - P_s\| \tag{7}$$

From Eq. (7), we can find that if there is no eccentricity of "ball 2" $(x_s = 0, y_s = 0)$, the angle-positioning error ε_z will have

no influence on the length change of the ball bar. Hence, ε_z cannot be identified without the eccentricity of "ball 2."

Equation (7) is used to map the relationship between the measured length change of the ball bar and the geometric errors of the rotary table. To identify the five position-dependent geometric errors, different installation parameters are selected to construct enough equations.

As shown in Fig. 1, three installation positions $\boldsymbol{P}_{c1}$, $\boldsymbol{P}_{c2}$, and $\boldsymbol{P}_{c3}$ are selected for tests. They are distributed on the circumference with radius of R, and the distance between the center of "ball 1" and the table surface is H_0. The initial position of "ball 1," $\boldsymbol{P}_{c1}$, $\boldsymbol{P}_{c2}$, and $\boldsymbol{P}_{c3}$, are set at $[R, 0, H_0]$, $[0, R, H_0]$, and $[0, -R, H_0]$ to simplify the installation procedure.

Two heights of "ball 2" from the table are utilized at each installation position $\boldsymbol{P}_c$ by the extension bar. The normal ball bar lengths are L_1 and L_2, respectively. The fixed positions of "ball 2" are $[0, 0, H_0 + H_1]$ and $[0, 0, H_0 + H_2]$, respectively.

Then, the identification model can be built through the five measurement results $[\Delta L_1(C), \Delta L_2(C), \Delta L_3(C), \Delta L_4(C)$, and $\Delta L_5(C)]$ and the geometric errors according to Eq. (7).

$$\begin{bmatrix} \frac{R}{\sqrt{H_1{}^2+R^2}} & 0 & \frac{-H_1}{\sqrt{H_1{}^2+R^2}} & 0 & \frac{(H_0+H_1)R}{\sqrt{H_1{}^2+R^2}} \\ \frac{R}{\sqrt{H_2{}^2+R^2}} & 0 & \frac{-H_2}{\sqrt{H_2{}^2+R^2}} & 0 & \frac{(H_0+H_2)R}{\sqrt{H_2{}^2+R^2}} \\ 0 & \frac{R}{\sqrt{H_1{}^2+R^2}} & \frac{-H_1}{\sqrt{H_1{}^2+R^2}} & \frac{-(H_0+H_1)R}{\sqrt{H_1{}^2+R^2}} & 0 \\ 0 & \frac{R}{\sqrt{H_2{}^2+R^2}} & \frac{-H_2}{\sqrt{H_2{}^2+R^2}} & \frac{-(H_0+H_2)R}{\sqrt{H_2{}^2+R^2}} & 0 \\ 0 & \frac{-R}{\sqrt{H_1{}^2+R^2}} & \frac{-H_1}{\sqrt{H_1{}^2+R^2}} & \frac{(H_0+H_1)R}{\sqrt{H_1{}^2+R^2}} & 0 \end{bmatrix} \begin{bmatrix} \delta_x \\ \delta_y \\ \delta_z \\ \varepsilon_x \\ \varepsilon_y \end{bmatrix} = \begin{bmatrix} \Delta L_1(C) \\ \Delta L_2(C) \\ \Delta L_3(C) \\ \Delta L_4(C) \\ \Delta L_5(C) \end{bmatrix} \tag{8}$$

Equation (8) can be simplified into the following form:

$$M_C E_C = M_L \tag{9}$$

$\boldsymbol{M}_C$ is the coefficient matrix, $\boldsymbol{E}_C$ defines the error vector, and $\boldsymbol{M}_L$ represents the measurement results.

The installation radius R of "ball 1" is optimized based on the sensitivity analysis of the coefficient matrix $\boldsymbol{M}_C$. The details are demonstrated in Section 4.1.

4 Analysis of testing scheme

4.1 Installation parameter optimization

The varieties of installation parameters R, H_1, H_2, and H_0 will disturb the coefficient matrix $\boldsymbol{M}_C$. This disturbance can be expressed as $\delta\boldsymbol{M}_C$ and then impact the identification results. Also, system errors in the double ball bar measurement system can cause the perturbation in vector $\boldsymbol{M}_L$. This perturbation can be represented as $\delta\boldsymbol{M}_L$. $\delta\boldsymbol{M}_C$ and $\delta\boldsymbol{M}_L$ will result in the change $\delta\boldsymbol{E}_C$ of the solution.

$$(M_C + \delta M_C)(E_C + \delta E_C) = M_L + \delta M_L \tag{10}$$

According to literature [28], the change rate of the solution can be expressed by the inequality in norm form.

$$\frac{\|\delta E_C\|}{\|E_C\|} \le \frac{\|M_C^{-1}\|\|M_C\|}{1-\|M_C^{-1}\|\|M_C\|\frac{\|\delta M_C\|}{\|M_C\|}} \left(\frac{\|\delta M_L\|}{\|M_L\|} + \frac{\|\delta M_C\|}{\|M_C\|} \right) \tag{11}$$

The coefficient matrix $\|M_C^{-1}\|\|M_C\|$ reflects the sensitivity of the solution with respect to the original data errors. It is also called the condition number. To simplify the calculation, the ∞ norm is selected to represent the condition number of the coefficient matrix $\boldsymbol{M}_C$.

$$cond(M_C) = \left\|M_C^{-1}\right\|_\infty \|M_C\|_\infty \tag{12}$$

The coefficient matrix $\boldsymbol{M}_C$ is determined by the installation parameters R, H_0, H_1, and H_2. The H_0 depends on the height of the socket, and it can only be adjusted within a small scale. Thus, H_0 is treated as a constant parameter in this paper. H_1 and H_2 are the vertical distance between "ball 1" and "ball 2" with two different rod lengths L_1 and L_2. H_1 and H_2 can be calculated as follows.

$$\begin{cases} H_1 = \sqrt{L_1{}^2 - R^2} \\ H_2 = \sqrt{L_2{}^2 - R^2} \end{cases} \tag{13}$$

In which L_1 and L_2 are the nominal lengths of the ball bar. Therefore, only parameter R can be easily changed during the measurement. Selecting a proper value for

parameter R to minimize the condition number of the matrix $\boldsymbol{M}_C$ can reduce the error influence resulted from the inaccuracy of the measured results and the installation location.

The condition number was evaluated with the change of R (the H_0 was set as 60 mm; the nominal length of the ball bar L_1 and L_2 was set as 150 mm and 300 mm, respectively).

As shown in Fig. 3, the condition number increases dramatically when the value of R closes to 0 mm or 150 mm. This is because when $R = 0$ mm or 150 mm, the cone test will be converted into the circular test, and the sensitivity of geometric error to the measurement results is changed hugely. Hence, greater fluctuations of the solution were produced. As the radius R added, the condition number decreases smoothly until $R = 136.5$. After that, it rises up again. Thus, there is an optimum value of R to achieve the minimum condition number.

4.2 Influence of the installation error of "ball 1"

Supposed that the installation error of "ball 1" is denoted as $\delta e_1 = (\delta e_{x1}, \delta e_{y1}, \delta e_{z1})$. Then, the actual initial position of "ball 1" is $(x_{c0} + \delta e_{x1}, y_{c0} + \delta e_{y1}, z_{c0} + \delta e_{z1})$.

Substituting the actual initial position coordinate into Eq. (7), take $x_s = 0$, $y_s = 0$, and $z_s = H_0 + H_{1(or2)}$, then the following equation can be obtained:

$$\begin{bmatrix} x_{c0} + \delta e_{x1} \\ y_{c0} + \delta e_{y1} \\ z_{c0} + \delta e_{z1} - (H_0 + H_{1(or2)}) \\ -(H_0 + H_{1(or2)})(y_{c0} + \delta e_{y1}) \\ (H_0 + H_{1(or2)})(x_{c0} + \delta e_{x1}) \end{bmatrix}^T \begin{bmatrix} \delta_x \\ \delta_y \\ \delta_z \\ \varepsilon_x \\ \varepsilon_y \end{bmatrix} = \Delta L(C) * \| P_c(C) - P_s \| \tag{14}$$

Additional sick length changes caused by installation errors of "ball 1" can be calculated as:

$$\begin{bmatrix} \delta e_{x1} \\ \delta e_{y1} \\ \delta e_{z1} \\ -(H_0 + H_{1(or2)})\delta e_{y1} \\ (H_0 + H_{1(or2)})\delta e_{z1} \end{bmatrix}^T \begin{bmatrix} \delta_x \\ \delta_y \\ \delta_z \\ \varepsilon_x \\ \varepsilon_y \end{bmatrix} / \| P_c(C) - P_s \| \tag{15}$$

The molecule in the formula is all second-order terms of small errors. Theoretically speaking, the molecule can be abandoned. In another word, the ball bar length variation is not sensitive to the installation errors of "ball 1."

To demonstrate the influence on ball bar length change caused by the installation errors of "ball 1," the PDGEs of the rotary axis are set as 0.05 mm/deg., H_0 is set as 60 mm, R is set as 135 mm, $H_1 = 65.384$ mm, and $H_2 = 267.909$ mm. The installation position of "ball 1" is (R, 0, H_0).

As shown in Fig. 4, after setting the PDGE as a fixed value, the additional ball bar length change is linearly proportional to the installation errors of "ball 1." The additional ball bar length change is less than 0.05 μm when the absolute value of installation error is less than 0.045 mm. Therefore, when the installation error of "ball 1" is controlled within a certain range, its influence on the identified results can be ignored. The installation errors of "ball 1" can only affect the original length of the ball bar with our method. The same conclusion can be summarized with setting the installation position of "ball 1" as (0, R, H_0) and (0, $-R$, H_0).

4.3 Influence of the positioning error of "ball 2"

The positioning error of "ball 2" is expressed as $\delta e_2 = (\delta e_{x2}, \delta e_{y2}, \delta e_{z2})$. Then, the actual position of "ball 2" is $x_s = \delta e_{x2}$, $y_s = \delta e_{y2}$, $z_s = H_0 + H_{1(or2)} + \delta e_{z1}$.

The additional ball bar length change due to the positioning error of "ball 2" can be obtained according to Eq. (7):

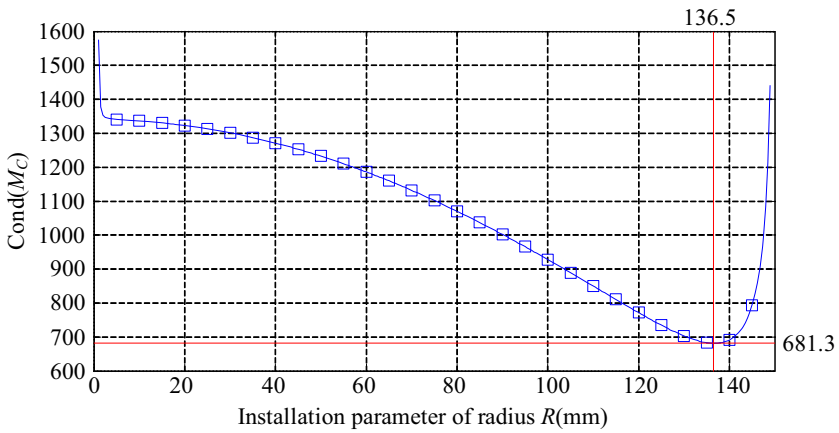

Fig. 3 Simulation results for the condition number influenced by the parameter R

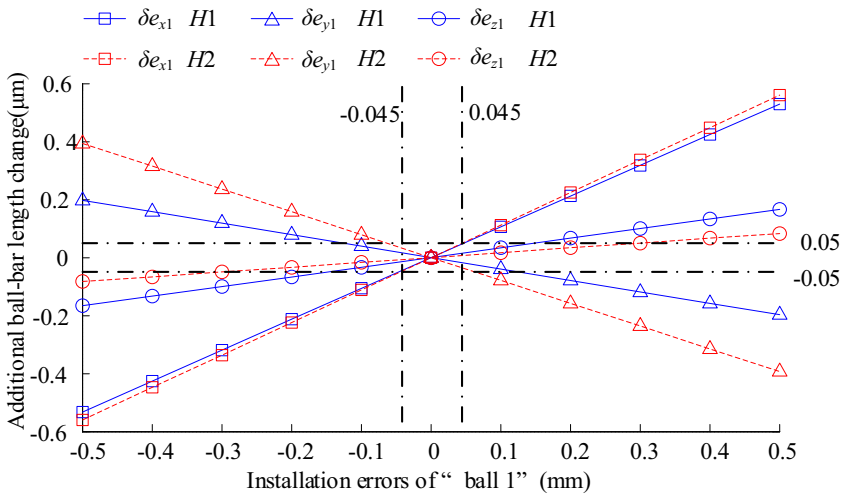

Fig. 4 Influence of installation errors of "ball 1" on additional ball bar length change

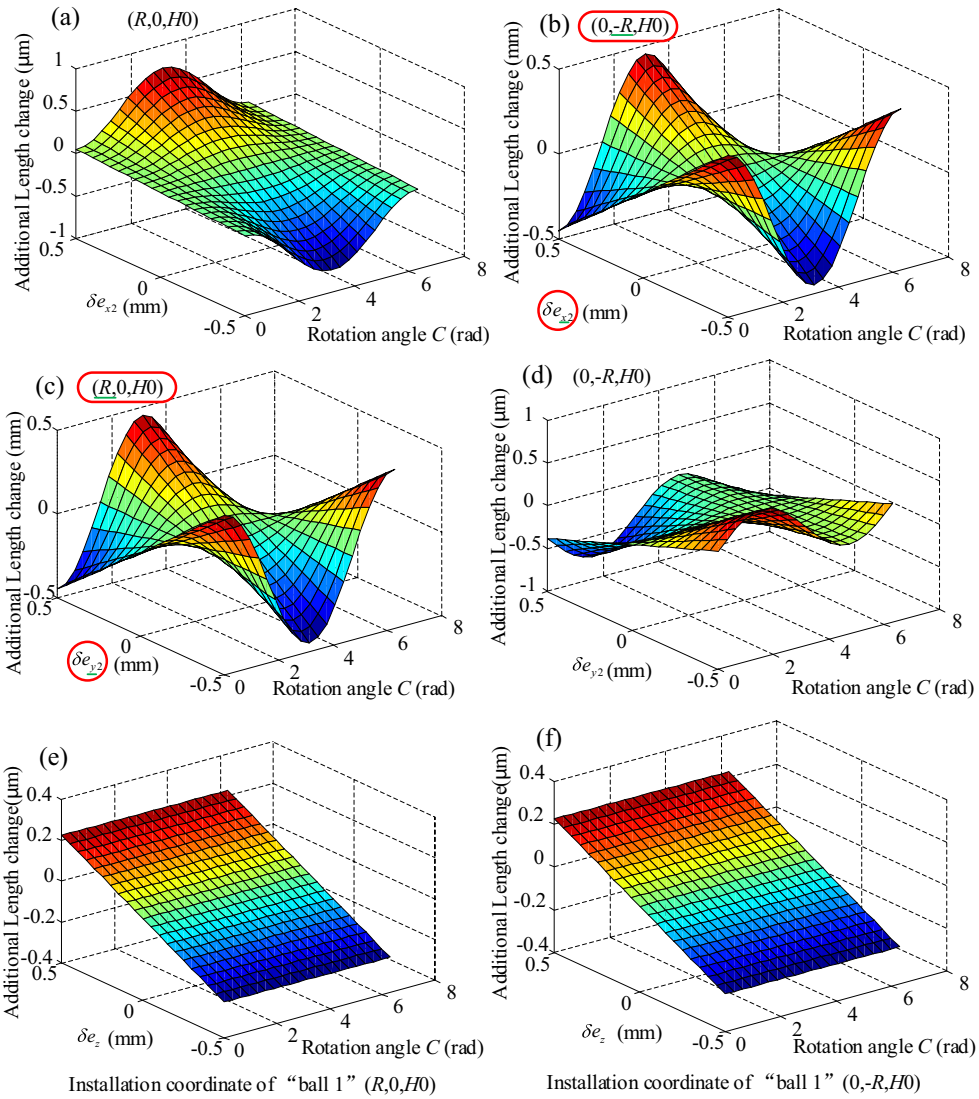

Fig. 5 Impact on the ball bar length change due to positioning errors of "ball 2"

Table 1 Standard uncertainty of the contributors

Contributor	Range	Standard uncertainty	Unit
Accuracy of ball bar	± 1	0.577	μm
Accuracy of indicator	± 3	1.732	μm
Setup error ΔR	± 5	2.887	μm
Errors ΔH_1, ΔH_2, and ΔH_0	± 3	1.732	μm

$$\begin{bmatrix} -\delta e_{x2}c_C - \delta e_{y2}s_C; \\ \delta e_{x2}s_C - \delta e_{y2}c_C; \\ -\delta e_{z2}; \\ \delta e_{y2}z_{c0}c_C - \delta e_{x2}z_{c0}s_C - \delta e_{z2}y_{c0}; \\ \delta e_{z2}x_{c0} - \delta e_{x2}z_{c0}c_C - \delta e_{y2}z_{c0}s_C; \\ \left(\delta e_{x2}y_{c0} - \delta e_{y2}x_{c0}\right)c_C + \\ \left(\delta e_{x2}x_{c0} + \delta e_{y2}y_{c0}\right)s_C \end{bmatrix}^T \begin{bmatrix} \delta_x \\ \delta_y \\ \delta_z \\ \varepsilon_x \\ \varepsilon_y \\ \varepsilon_z \end{bmatrix} / \|P_c(C) - P_s\| \quad (16)$$

From Eq. (16), the rotation positioning error ε_z and the rotation angle C can also affect the length change of ball bar. Same as Section 4.2, the PDGEs of rotary axis are set as 0.05 mm/deg., H_0 is set as 60 mm, R is set as 135 mm, and $H_1 = 65.384$ mm. And the influence on additional ball bar length change due to positioning error of "ball 2" is displayed in Fig. 5. The additional ball bar length change is impacted by the positioning error of "ball 2," rotation angle C, and the installation location of "ball 1." The additional ball bar length change is sensitive to the positioning error in x and y direction and is insensitive to the positioning error in z direction. Little impact occurs when the direction of radial positioning error is in accordance with the direction of the installation location of "ball 1," see in Fig. 5a, d. Contrarily, see in Fig. 5b, c, when the direction of radial positioning error is vertical to the direction of the installation location of "ball 1," there will have big impact on the measurement results. The same conclusion of $H_2 = 267.909$ mm can be summarized and was not displayed here.

4.4 Uncertainty analysis

It is important to investigate the standard uncertainty of the measured errors to ensure their confidence intervals. From $M_C E_C = M_L$, vector $\boldsymbol{E}_c$ can be derived as follows:

$$E_C = M_C^{-1} M_L \quad (17)$$

Expanding Eq. (17), the PDGEs can be derived as a relationship about ΔL, R, H_0, H_1, and H_2. Hence, the indirect combined standard uncertainties of the identified PDGEs can be calculated according to the uncertainty transfer formula. And the standard uncertainties of the double ball bar, the installation and the positioning errors ΔR, ΔH_0, ΔH_1, and ΔH_2, affect the standard uncertainty of identified PDGEs. The standard uncertainty of ΔL is determined by the accuracy of double ball bar. And the standard uncertainties of R, H_0, H_1, and H_2 are determined by the positioning accuracy of translational axes and the dial indicator which is used to define the position of the axis line of the rotary table. All contributors to the measured PDGEs are ranged by measurement and experience, and the standard uncertainties of those contributors are listed in Table 1 by assuming a rectangular distribution.

The geometric errors of the other axes do not affect the standard uncertainty of the identified PDGEs because only rotary axis C is driven during measurement. Then uncertainties of the identified PDGEs are summarized in Table 2 according to the calculation method of combined uncertainty. It can be found that the uncertainties of measured PDGEs are really small by reducing the uncertainty contributor.

5 Measurement and verification experiment

Measurement and verification tests by the proposed method were conducted on a five-axis machine tool. The machine tool structure can be found in the published papers [29]. The test instrument is QC10-H42116 obtained from Renishaw with the resolution of 0.1 μm and the accuracy of ± 1 μm (20 °C).

5.1 Measurement step

Firstly, the coordinate origin of IFCS was calibrated, and the absolute coordinate system for measurement was set on the center of the upper surface of the table. The rotation axis was calibrated using the dial indicator.

Secondly, the magnetic socket was installed. The magnetic socket was roughly adsorbed on the location of ($X = R$, $Y = 0$) in the IFCS, and the fastening bolt on the magnetic socket was

Table 2 Uncertainties of measured PDGEs

PDGEs	Standard uncertainty	Coverage factor	Measurement uncertainty	Unit
δ_x	1.67	2	3.34	μm
δ_y	1.67	2	3.34	μm
δ_z	2.65	2	5.3	μm
ε_x	13.29	2	26.58	μrad
ε_y	13.29	2	26.58	μrad

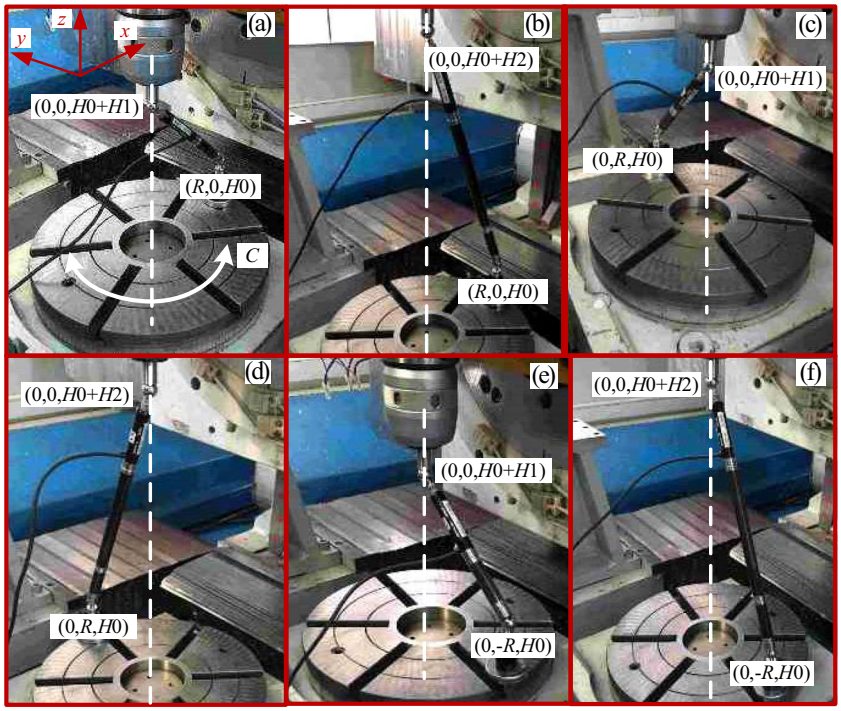

Fig. 6 The measurement experiment

loosened for the activity within a certain range. Then the spindle cup was positioned to the location ($X = R$, $Y = 0$) precisely. After that, the Z-axis was driven to adsorb the "ball 1" slowly in the magnetic socket on the rotary table. The Z coordinate at this time was recorded as the height H_0 of "ball 1", and the fastening bolts were locked. In this section, $H_0 = 60$ mm.

Thirdly, spindle was moved to the coordinate (0, 0, $sqrt(L^2-R^2) + H_0$), and the two balls were adsorbed in the magnetic cups linked by the ball bar, where L denotes the nominal length of the ball bar and R denotes the installation parameter of the magnetic socket on the table surface. In this section, $L = 150$ and 300 mm, $R = 135$ mm.

Then, the test code was written and executed on the machine tool; only rotation C-axis was driven. The length change of double ball bar was collected with ten tests. Finally, the installation locations of the magnetic socket on the table surface were adjusted to (0, R, H_0) and (0, $-R$, H_0). Similarly, the tests were conducted with two different ball bar nominal lengths, and measurement results of the ten tests were gathered repeatedly. The six testing procedures are shown in Fig. 6. The machine tool had been warmed up, and the entire measuring process did not take long; hence, the effect of thermal error was ignored.

5.2 Validation of error identification results

The identified PDGEs were displayed as shown in Fig. 7. It can be seen that the angular errors ε_x and ε_y were relatively

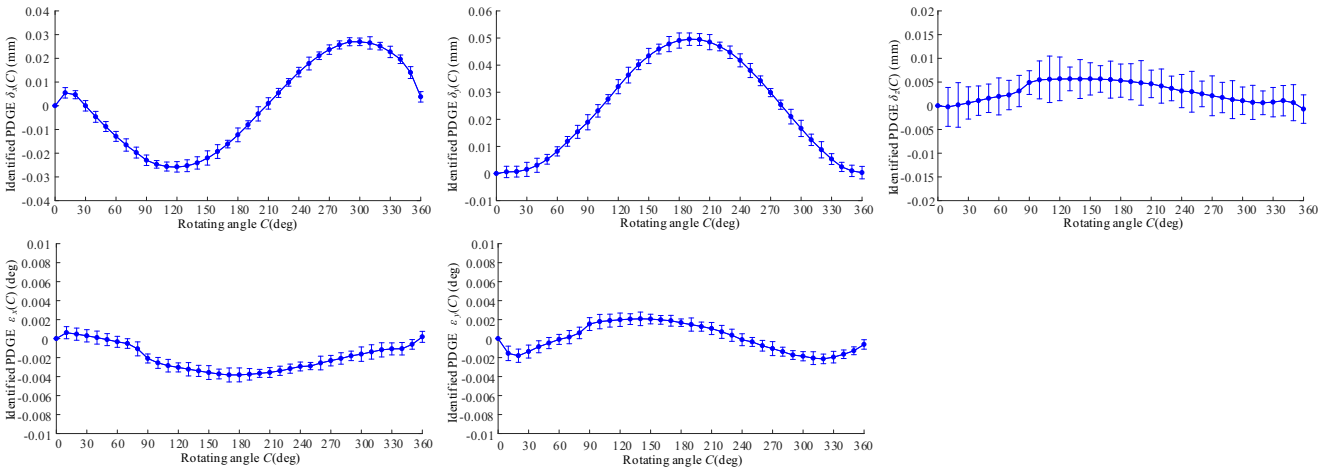

Fig. 7 Identified results of PDGEs

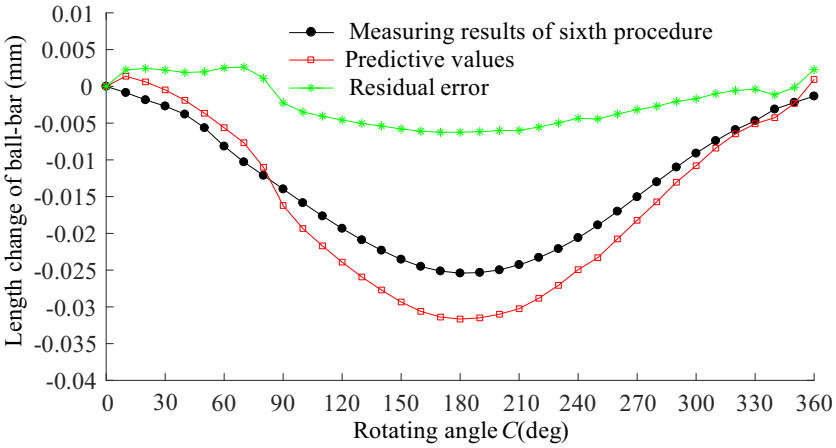

Fig. 8 Comparison of measuring results and predictive values

small. The axial error δ_z is smaller than the radial errors δ_x and δ_y.

According to Eq. (8), five groups of measurement results can be used to identify the five PDGEs. The sixth measurement results were used to verify the effectiveness of the proposed method. As shown in Fig. 8, the measuring results were almost consistent with the predictive values which were calculated by the identified geometric errors and Eq. (8).

In order to further verify the advancement of this method, error compensation tests using the third and fourth procedures (see in Fig. 6c, d) were conducted. The identified five PDGEs can be easily transferred to the positional errors in three coordinate axes according to Eq. (4), i.e., Δx_c, Δy_c, and Δz_c. And these three errors can be compensated by moving the three translational axes during ball bar test. The ball bar length change before and after compensation is depicted in Fig. 9. The uncertainty was increased with the movements of translational axes, although the errors of translational axes were compensated during the test. Moreover, the angular positioning error ε_z was not identified and compensated. Hence, the compensation accuracy was impacted. However, the ball bar length change was decreased significantly after compensation. The comparison results in Fig. 8 and the compensation results in Fig. 9 indicate that the proposed measurement method can effectively identify the PDGEs of the rotary table.

6 Conclusions

A method to identify the PDGEs of rotary axis with only single-axis driven was proposed. The cone test trajectory using double ball bar was designed effectively to measure and identify the PDGEs. Error identification model was built according to the basic installation parameters and the measured length change of double ball bar. Besides, the installation parameter R was optimized by the condition number of coefficient matrix to ensure the stability of identified results. The uncertainty of the identified results was small through single-axis driven. To further improve the accuracy and stability, error data behavior analysis and decomposition tracing method based on big data-driven will be studied in the future.

Sensitivity of the installation errors was analyzed with our proposed measurement method. It showed that the installation errors of “ball 1” in the magnetic socket on rotary table had

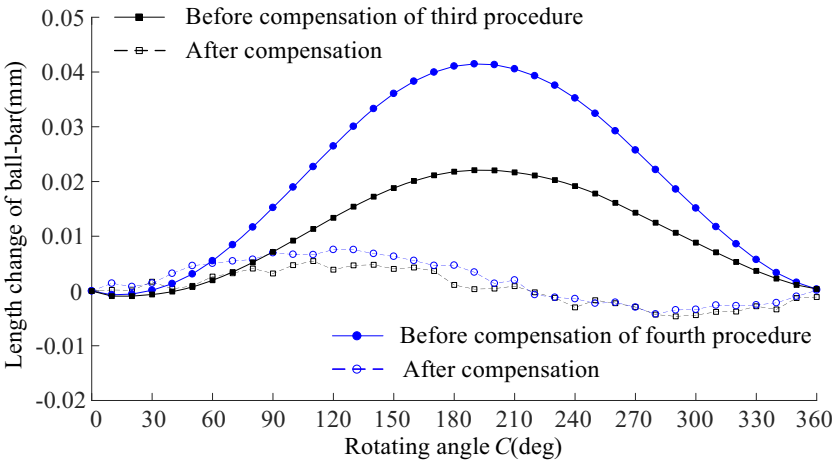

Fig. 9 Length change of ball bar before and after compensation

little impact on the identified results. On the contrary, the identified results were greatly impacted by the installation errors of "ball 2" on spindle, especially the radial positioning error (x and y direction for rotary C-axis). Especially, biggest influence of positioning error in x direction was found when "ball 1" was installed in the coordinates $(0, R, H_0)$ and $(0, -R, H_0)$, and at these tests, the positioning error in x direction needs more attention than that in y direction. Similarly, biggest influence of positioning error in y direction was found when "ball 1" was installed in $(R, 0, H_0)$.

Funding information This work is supported by the National Natural Science Foundation of China (Grant no. 51635003) and is funded by the Research Fund of DMIECT (Grant no. DM201701).

References

1. Moriwaki T (2008) Multi-functional machine tool. CIRP Ann Manuf Technol 57(2):736–749
2. Zhang Y, Yang JG, Zhang K (2013) Geometric error measurement and compensation for the rotary table of five-axis machine tool with double ballbar. Int J Adv Manuf Technol 65:275–281
3. Wang JD, Guo JJ, Zhou BQ, Xiao J (2012) The detection of rotary axis of NC machine tool based on multi-station and time-sharing measurement. Measurement 45:1713–1722
4. Zhang ZJ, Ren MJ, Liu MJ, Wu XM, Chen YB (2015) A modified sequential multilateration scheme and its application in geometric error measurement of rotary axis. Procedia CIRP 27:313–317
5. Jiang ZX, Song B, Zhou XD, Tang XQ, Zheng SQ (2015) Single setup identification of component errors for rotary axes on five-axis machine tools based on pre-layout of target points and shift of measuring reference. Int J Mach Tools Manuf 98:1–11
6. Ibaraki S, Ota Y (2014) A machining test to calibrate rotary axis error motions of five-axis machine tools and its application to thermal deformation test. Int J Mach Tools Manuf 86:81–88
7. Ibaraki S, Iritani T, Matsushita T (2012) Calibration of location errors of rotary axes on five-axis machine tools by on-the-machine measurement using a touch-trigger probe. Int J Mach Tools Manuf 58:44–53
8. Huang ND, Zhang SK, Bi QZ, Wang YH (2016) Identification of geometric errors of rotary axes on 5-axis machine tools by on-machine measurement. Int J Adv Manuf Technol 84(1–4): 505–512
9. Ibaraki S, Iritani T, Matsushita T (2013) Error map construction for rotary axes on five-axis machine tools by on-the-machine measurement using a touch-trigger probe. Int J Mach Tools Manuf 68:21–29
10. He ZY, Fu JZ, Zhang LC, Yao XH (2015) A new error measurement method to identify all six error parameters of a rotational axis of a machine tool. Int J Mach Tools Manuf 88:1–8
11. Ibaraki S, Oyama C, Otsubo H (2011) Construction of an error map of rotary axes on a five-axis machining center by static R-test. Int J Mach Tools Manuf 51:190–200
12. Hong CF, Ibaraki S, Oyama C (2012) Graphical presentation of error motions of rotary axes on a five-axis machine tool by static R-test with separating the influence of squareness errors of linear axes. Int J Mach Tools Manuf 59:24–33
13. Lau K, Ma Q, Chu X, Liu Y, Olson S (1999) An advanced 6-degree-of-freedom laser system for quick CNC machine and CMM error mapping and compensation. WIT Trans Eng Sci 23: 421–434
14. Chen DJ, Dong LH, Bian YH, Fan JW (2015) Prediction and identification of rotary axes error of non-orthogonal five-axis machine tool. Int J Mach Tools Manuf 94:74–87
15. Xiang ST, Yang JG, Zhang Y (2014) Using a double ball bar to identify position-independent geometric errors on the rotary axes of five-axis machine tools. Int J Adv Manuf Technol 70:2071–2082
16. Zargarbashi SHH, Mayer JRR (2006) Assessment of machine tool trunnion axis motion error, using magnetic double ball bar. Int J Mach Tools Manuf 46:1823–1834
17. Lei WT, Sung MP, Liu WL, Chuang YC (2007) Double ballbar test for the rotary axes of five-axis CNC machine tools. Int J Mach Tools Manuf 47:273–285
18. Lee KI, Yang SH (2013) Accuracy evaluation of machine tools by modeling spherical deviation based on double ball-bar measurements. Int J Mach Tools Manuf 75:46–54
19. Tsutsumi M, Saito A (2004) Identification of angular and positional deviations inherent to 5-axis machining centers with a tilting-rotary table by simultaneous four-axis control movements. Int J Mach Tools Manuf 44:1333–1342
20. Zhu SW, Ding GF, Qin SF, Lei J, Zhuang L, Yan KY (2012) Integrated geometric error modeling, identification and compensation of CNC machine tools. Int J Mach Tools Manuf 52:24–29
21. Chen JX, Lin SW, He BW (2014) Geometric error measurement and identification for rotary table of multi-axis machine tool using double ballbar. Int J Mach Tools Manuf 77:47–55
22. Chen JX, Lin SW, Zhou XL, Gu TQ (2016) A ballbar test for measurement and identification the comprehensive error of tilt table. Int J Mach Tools Manuf 103:1–12
23. Jiang XG, Cripps RJ (2015) A method of testing position independent geometric errors in rotary axes of a five-axis machine tool using a double ball bar. Int J Mach Tools Manuf 89:151–158
24. Lee KI, Yang SH (2013) Robust measurement method and uncertainty analysis for position-independent geometric errors of a rotary axis using a double ball-bar. Int J Precis Eng Manuf 14(2):231–239
25. Lee KI, Yang SH (2013) Measurement and verification of position-independent geometric errors of a five-axis machine tool using a double ball-bar. Int J Mach Tools Manuf 70:45–52
26. Xiang ST, Yang JG (2014) Using a double ball bar to measure 10 position-dependent geometric errors for rotary axes on five-axis machine tools. Int J Adv Manuf Technol 75:559–572
27. Ding S, Huang XD, Yu CJ, Liu XY (2016) Identification of different geometric error models and definitions for the rotary axis of five-axis machine tools. Int J Mach Tools Manuf 100:1–6
28. Golub GH, VanLoan CF (2012) Matrix computations, 4th edn. Johns Hopkins University Press, Maryland
29. Ding S, Huang XD, Yu CJ, Liu XY (2016) Novel method for position-independent geometric error compensation of five-axis orthogonal machine tool based on error motion. Int J Adv Manuf Technol 83(5):1069–1078